THE PUBLISHING HOUSE
OF THE ROMANIAN ACADEMY

*PROCEEDINGS OF THE ROMANIAN ACADEMY, Series A,*
*Volume 20, Number 1/2019, pp. 29–36*

**PHYSICS**

# RADIOCHROMIC FILM CALIBRATION AT 9 MV ACCELERATOR OF IFIN-HH

A. S. CUCOANES[1], M. GUGIU[1,2], F. ROTARU[1,2], F. NEGOITA[1,2], L. TUDOR[1,3], S. KISYOV[1], C. MANAILESCU[2], V. NASTASA[1,4]

[1]ELI-NP, "Horia Hulubei" National Institute for Physics and Nuclear Engineering, 30 Reactorului Str., 077125 Magurele, Romania
[2]"Horia Hulubei" National Institute for Physics and Nuclear Engineering, 30 Reactorului Str., 077125 Magurele, Romania
[3]University Politehnica of Bucharest, 313 Splaiul Independentei, 060042 Bucharest, Romania
[4]National Institute for Laser Plasma and Radiation Physics, 409 Atomistilor Str., 077125 Magurele, Romania
Corresponding author: Andi S. CUCOANES, E-mail: andi.cucoanes@eli-np.ro

**Abstract:** It is now experimentally proven that intense beams of protons are generated in interactions between high power lasers and thin solid targets. The energy spectrum and divergence of such beams can be measured with stack structured calorimeters based on Radiochromic films (RCF). However, in order to provide useful information, RCF have to be calibrated by a relation between the radiation dose that hits them and the colour change consequently recorded. We report here an experiment performed at the 9 MV Tandem accelerator of IFIN-HH, having as aim the calibration of two new RCF types: HD-V2 and MD-V3 produced by Ashland Inc. [1] to MeV protons. Although proton calibration data exists in literature for HD-V2 [2,3], we found no references for calibration of MD-V3 with this type of particles. Our method is able to provide a global view on the RCF response from the variation of the radiation dose given by the angular dependence of the scattering cross-section of a proton beam on a thin target.

***Key words*:** Radiochromic films, calibration, high power laser, ELI-NP.

## 1. INTRODUCTION

Ultra-intense laser-plasma interactions, beyond $10^{18}$ W/cm$^2$, are able to release dense bunches of accelerated particles such as light ions, electrons and gamma rays. For example, a laser accelerated proton beam has broad energy spectrum, large angular distribution, and integrated charge up to 1 μC per pulse. Consequently, it can be used for various applications going from the production of medical radioisotopes [4] to new technologies for space applications [5] and management of nuclear waste disposals [6], all of them requiring an excellent characterization of the beam properties.

Among the experimental devices able to provide such type of information, stack structures based on passive detectors such as RCF or Imaging Plates (IP) are often used for the measurement of the energy spectrum and divergence [7]. The principle is rather simple: ions with different energies are stopped at different depths in the stack thus each layer will contain mostly depositions from a specific energy range, more precisely where the Bragg peak is localized. Further, the proton spectrum and divergence can be reconstructed from data provided by RCF scans, as described briefly in the last part of this paper. However, in order to be used in stack detectors, RCF have to be calibrated in terms of ionizing radiation, for the same conditions as for the laser-plasma experiments, meaning the same scanning technique, the same generation of films, etc.

## 2. RADIOCHROMIC FILMS

RCF are self-developing plastic films composed by an active (sensitive) layer of emulsion and one or more base layers of polyester acting as substrate. This type of detectors are extensively used in clinical dosimetry and are continuously subject of improvements in their structure and material, having as result an

increase of sensitivity. RCF are self-developing plastic films composed by an active (sensitive) layer of emulsion and one or more base layers of polyester acting as substrate. These types of detectors are extensively used in clinical dosimetry and are continuously subject of improvements in their structure and material, having as result an increase of sensitivity.

When irradiated, the active layer undergoes a polymerization reaction [8] having as consequence a colour change of the film. The parameter:

$$OD = \log\left(\frac{PV_{\max} - PV_{sig}}{PV_{\max} - PV_{bkg}}\right) \tag{1}$$

called Optical Density (OD), characterizes the colour or grayscale change of the scanned RCF images. It is a function of the pixel values of irradiated ($PV_{sig}$) and non-irradiated ($PV_{bkg}$) regions as well as the maximum pixel value ($PV_{max}$) which depends of the scan resolution.

The excellent properties of the RCF detectors such as high spatial resolution, good dose sensitivity and reproducibility, insensitivity to the electromagnetic noise (a major concern in laser-plasma experiments at very high intensity), make them suitable for several applications, notably the detection of the laser based accelerated ions. In this perspective, RCF based detectors are suitable for single shot use, although systems which measure particles from few shots could also be imagined [9]. As a downside, RCF are unable to discriminate between different types of ionizing particles.

In our analysis we considered two RCF types: HD-V2 and MD-V3, both foreseen to be used in experiments planned at ELI-NP [10]. HD-V2 has a 8μm active layer deposed on a 97 μm polyester substrate while MD-V3 has a 15 μm active layer placed in a sandwich like structure between two 120 μm polyester substrates. The dose ranges are 10 Gy to 1 kGy for HD-V2 and respectively 1 to 100 Gy for MD-V3. Although not specified in the technical documentation, we assumed for all layers of both types a mean density of 1.36 g/cm$^3$ [3], a value close to the Mylar density.

The response of HD-V2 films has been analysed for alpha particles from an $^{241}$Am source in [11], for 10 MeV photons in [12] and for protons different energies in [2,3], however for MD-V3, we found no calibration data for MeV protons in the literature.

## 3. EXPERIMENTAL SETUP

Our experiment is based on the relation between the scattering cross-section of a proton beam on a thin Tantalum foil and the RCF response. We used protons provided by the 9 MV Tandem accelerator of IFIN-HH [13]; the experimental setup is shown in Fig. 1.

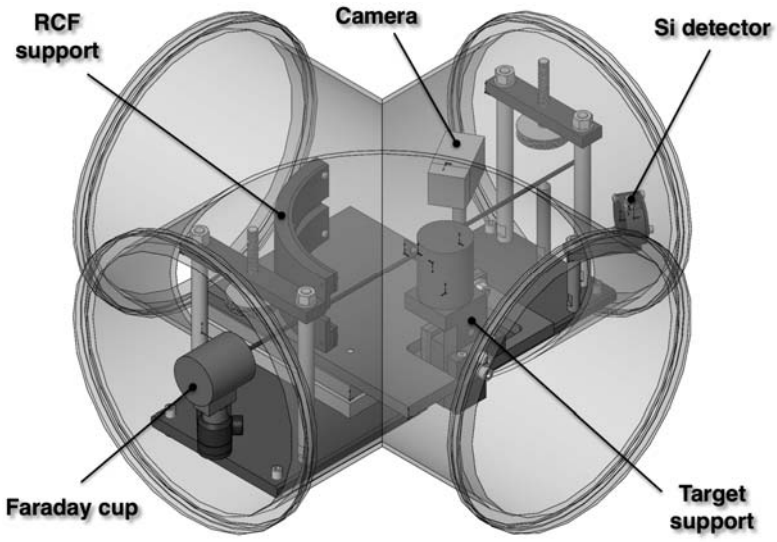


Fig. 1 – The experimental setup. The interaction chamber is a DN200 ”cross”, the red line is the collimated proton beam. Other elements are explained in text.

The incoming beam is collimated by 2 sets of slits with small aperture (approx. 2 mm) placed at more than 1 m one from each other, previously to the entrance in the interaction chamber. The target support could be moved on vertical direction, allowing four target distinct positions. One of them corresponds to the target placed on the proton beam direction. Another position lets the beam not scattered, in order to be measured with a Faraday cup placed at 0 degrees, as shown in Fig.1. The remaining two positions let the beam hit a small RCF piece placed on the target support aiming to provide an estimation of the beam size and position and respectively a phosphorous screen attached also to the target support which allowed the beam visualization on a camera. During the irradiation, a Si based detector recorded the scattered proton flux in the backward direction, monitoring the beam stability.

The RCF stack was covered with an Al foil and was placed on a curved Al support which assured the same distance to the interaction point: 100 mm. The target thickness, 44 μm, has been measured in the irradiated region with ±5 μm precision.

Due to cross section variation with the scattering angle, various doses were delivered on the RCF surface for a given set of experimental conditions (beam intensity, measuring time, etc.). The RCF support was attached to a removable table (dark-orange in Fig.1) with kinematic feature for precise repositioning. The RCF support covers scattering angles starting from 10 degrees and allows that a portion of the RCF stack to be unexposed to the radiation, for background measurement (demanded by Eq.1). The horizontal and vertical alignment of the setup has been checked before and after the experiment.

## 4. DATA ANALYSIS

Each irradiated RCF (Fig. 2) was scanned in 16 bits grayscale at 600 dpi on a Epson V850 scanner in transmission mode. The profiles over the irradiated surface were extracted using ImageJ [14] and further data analysis was done in ROOT [15].

Fig. 2 – The experimental setup. The interaction chamber is a DN200 “cross”,
the red line is the collimated proton beam. Other elements are explained in text.

We based our data analysis on a grid of angular values for which we estimated the dose, we computed OD according to Eq.1 and we propagated the uncertainties as described in the following section of this paper. The energy depositions of protons in target and RCF layers has been estimated with SRIM [16] and the cross-section of the beam scattering inside the target with the Rutherford formalism for elastic scattering [17]. The angle values have been corrected for the beam shift using the expression:

$$\mathrm{F_c}\left(\theta,\mathrm{d}\right)=\arctan\left(\frac{\sin\theta}{\cos\theta+\mathrm{d}/\mathrm{R}}\right), \tag{2}$$

where θ is the scattering angle, $d$ is the deviation of the beam center in the horizontal plane and $R$ is the radius of the circle defined by the RCF support.

Table 1 shows a summary of the analyzed runs containing the proton beam characteristics (energy, intensity, radius), the stack structure and the irradiation time, measured with second precision.
The estimated energy range of protons at the target’s rear side is shown in Fig. 3. The wiggles are given by the spatial resolution of the energy depositions considered in our estimation.

*Table 1*

Experimental parameters of the analyzed runs: type and number of layers in the stack,
energy and current of the incident beam on the target, beam half size and irradiation time

| RCF | Layers | $E_p$[MeV] | $I_p$[nA] | $r_b$[mm] | Time[$\cdot 10^3$s] |
|---|---|---|---|---|---|
| HD-V2 | 7 | 10 | 1 | 1.9 | 14.45 |
| MD-V3 | 3 | 10 | 1 | 1.4 | 7.24 |

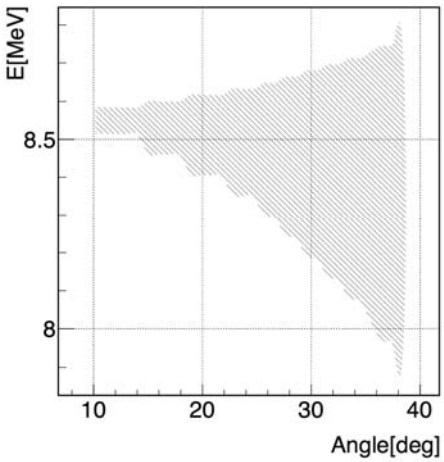


Fig. 3 – Proton energies at target rear side as function of scattering angle from a 10 MeV incoming beam. For a given scattering angle, the grey region ranges between the energies corresponding to scattering at the target front (lower edge) and rear (upper edge) side.

### 4.1. Sources of uncertainty

In our analysis we identified several sources of incertitude associated to both OD and estimated dose.

We propagated 3% uncertainty given by the target thickness measurement on the estimated dose for each scattering angle as shown for the HD-V2 run in Fig. 4-left. The dark blue line represents the uncertainty associated to the last layer in the stack, close to the Bragg peak, for which the impact of this uncertainty is most important due to strong fluctuations of the deposited energy.

We computed the deviation generated by the beam diameter on the scattering angle as [$F_c(\theta, r_b)$, $F_c(\theta,-r_b)$] using the expression from Eq. 2 and $r_b$ is the proton beam half size in the horizontal plane. We propagated this deviation on the estimated dose obtaining results as shown in Fig. 4-right for HD-V2 run. We notice a decrease of this uncertainty with the scattering angles, most important for the deepest layer in the stack.

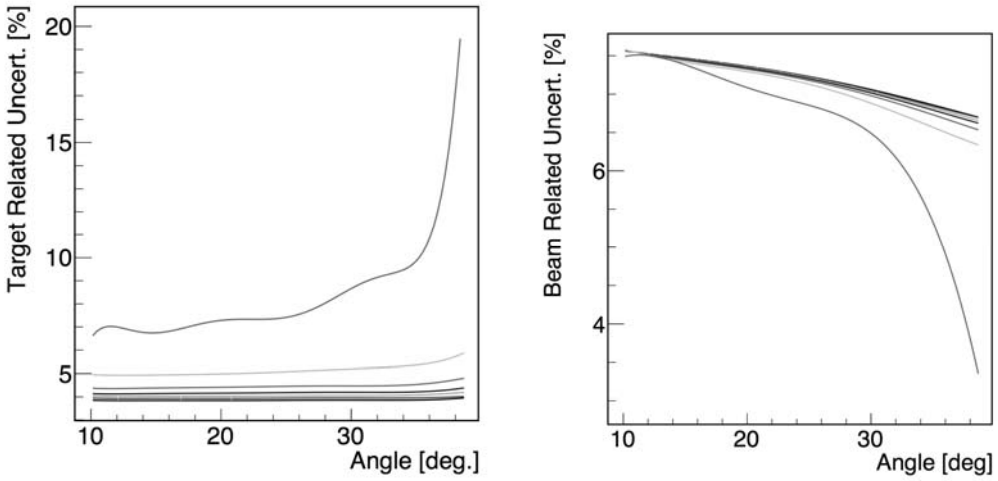


Fig. 4 – Angular dependence of the target thickness and beam diameter related uncertainties for HD-V2 run. Each color corresponds to a layer in the stack, where the following color scheme has been chosen from the first to the last layer: black, red, green, blue, magenta, cyan and dark blue.

We have also estimated the variation of the integrated dose over the whole runtime by analyzing the number of counts recorded by the Si detector and we obtained 10 % relative uncertainty.

As regarding the OD systematics we consider two contributions. As one of them, we introduced the relative uncertainty given by the averaged OD values for integer scattering angles given by:

$$\delta_{aa} = \delta_{\overline{OD}} = \frac{\sqrt{\sum_i \left(OD_i - \overline{OD}\right)^2}}{\sum_i OD_i} \tag{3}$$

As another contribution, measuring the fluctuations of the pixel values in the non-irradiated regions we determined 2 % relative uncertainty on the background subtraction that, propagated in Eq.1, results in 1.23% relative uncertainty on OD values.

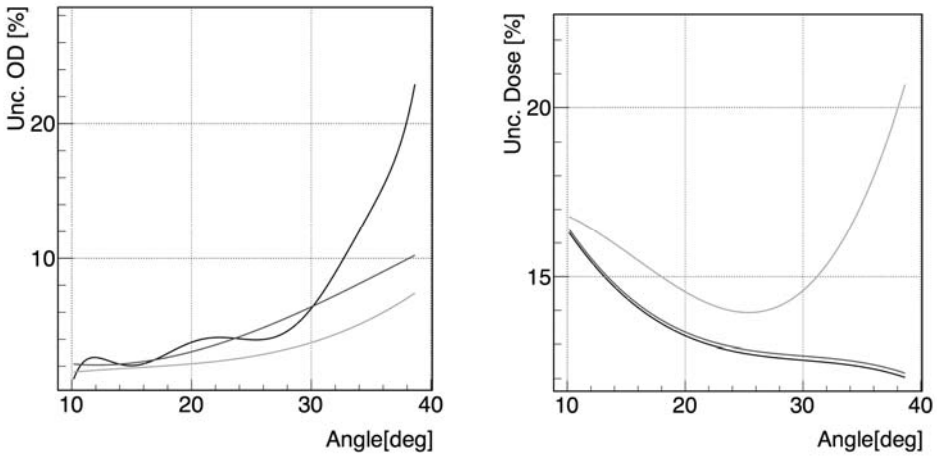


Fig. 5 – Angular dependence of the total Optical Density (left) and Dose (right) related uncertainties for MD-V3 run. Each color corresponds to a layer in the stack, where the following color scheme has been chosen from the first to the last layer: black, red and green.

The total systematic error is computed by adding in quadrature the previous described components. In consequence we assume for OD:

$$\delta_{tot}^{OD} = \sqrt{\delta_{aa}^2 + \delta_{bk}^2} \tag{4}$$

and for the estimated dose:

$$\delta_{tot}^{DO} = \sqrt{\delta_{tt}^2 + \delta_{bd}^2 + \delta_{id}^2} \tag{5}$$

where $\delta_{xx}$ are the induced uncertainties for: average scattering angle (*aa*), background subtraction (*bk*), target thickness (*tt*), beam diameter (*bd*) and integrated dose (*id*) respectively. We show in Fig. 5 the total errors related to OD and estimated dose for the MD-V3 run.

### 4.2. Discussion of results

In our analysis we computed the energy deposition in the active layer, dose and the optical density of each RCF layer in the stack. These quantities are represented in Fig. 6 for both, HD-V2 and MD-V3 runs. We noticed the increase of the energy deposition in the active layer with the depth as the energy loss increases with the stack thickness, but also with the scattering angle. The energy loss increases with the effective path of the protons inside the target, thus with the scattering angle. The combination of these effects has as consequence important energy depositions for the last layer in the stack at big angles. By comparing HD-V2 and MD-V3 runs, the difference between the energy depositions is a result of different depths in the stack and different thicknesses of the sensitive layers.

The same effects are also present in the dose estimation (middle plots in Fig. 6). In this case, the dominant effect is the decrease of the proton flux with the scattering angle as a consequence of the scattering cross-section variation.

The same effects are also present in the dose estimation (middle plots in Fig. 6). In this case, the dominant effect is the decrease of the proton flux with the scattering angle as a consequence of the scattering cross-section variation.

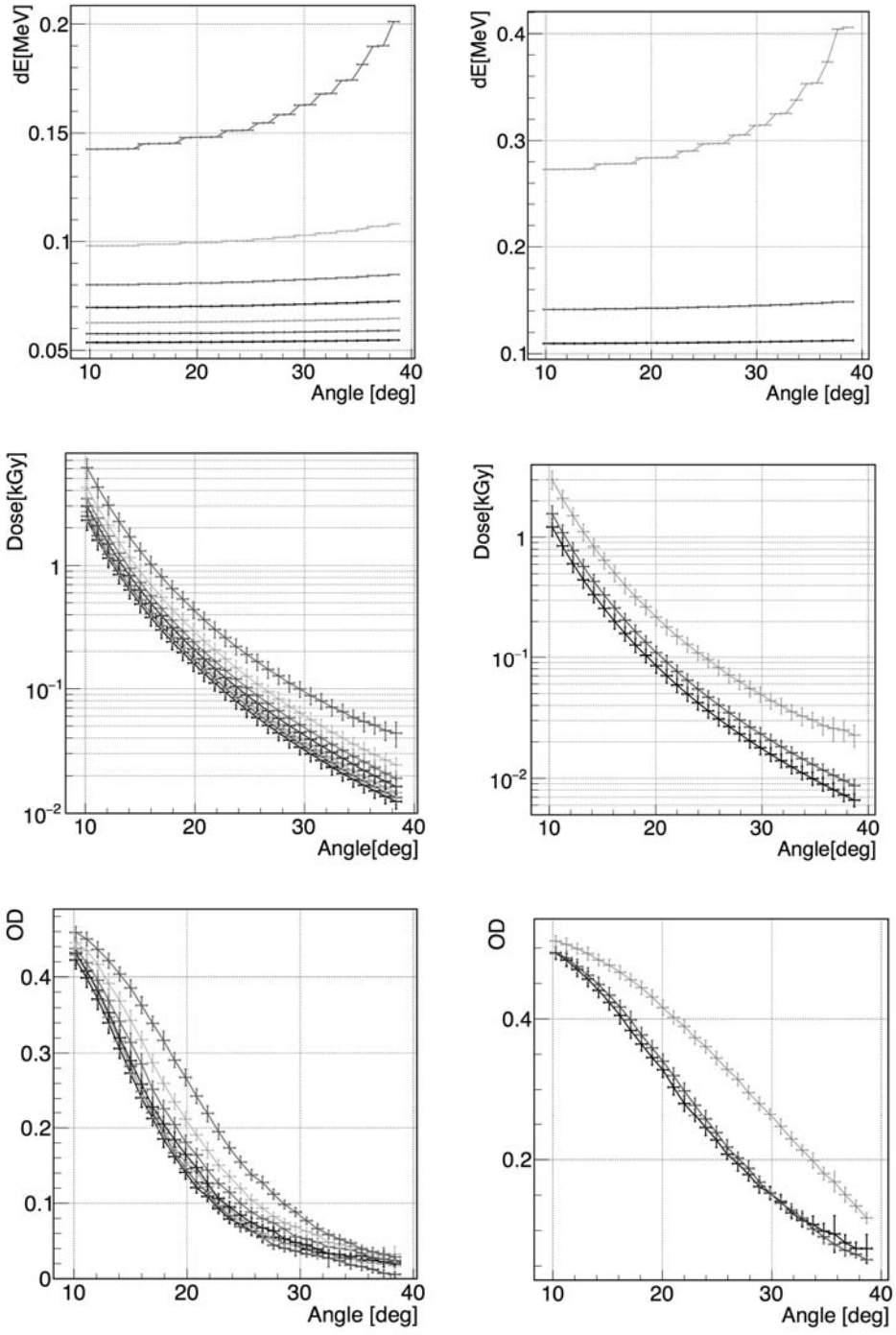


Fig. 6 – Angular dependence of the energy deposition in the active layer (up), total dose (middle) and Optical Density (down) for HD-V2 (all left) and MD-V3 (all right) stacks given the runs summarized in Table1. Each color represents a layer in the stack, with the same convention for both stacks. Starting from the first to the last layer, the color convention is: black, red, green, blue, magenta, cyan and dark-blue.

In order to deliver functional expressions of the calibration curves, we combined data from all layers, as shown in Fig. 7. Here, the total dose versus optical density was fitted with a 3-th order polynomial function:

$$F(OD) = \sum_i a_i OD^i \tag{6}$$

and we extracted the coefficients from in Table 2. The plots in Fig. 7 show also the evolution of the RCF response close to saturation and close to the low dose region.

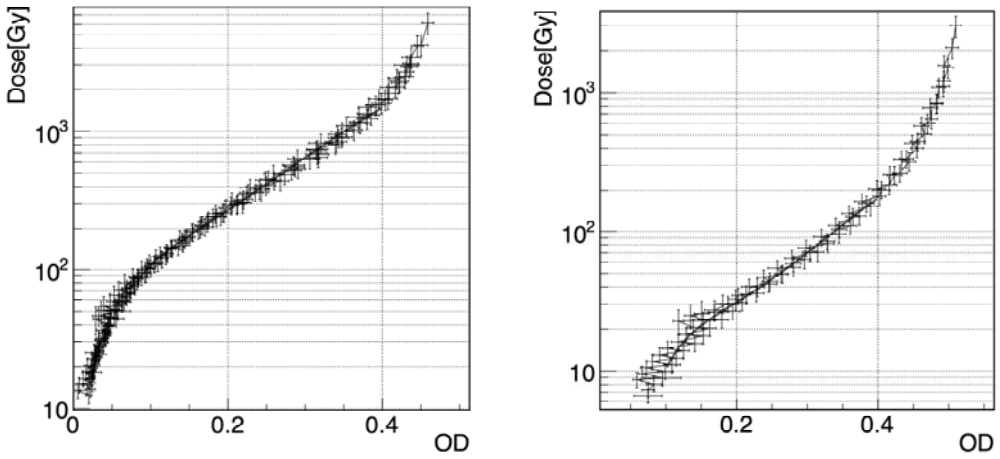


Fig. 7 – Global fits on data from all layers of HD-V2 (all left) and MD-V3 (all right) stacks.

*Table 2*

Functional parameters obtained from fits with Eq. 6 on the plots shown in Fig. 7

| RCF | $a_0$ | $a_1$ | $a_2$ | $a_3$ | $\chi^2$/ndf |
|---|---|---|---|---|---|
| HD-V2 | -91.54 | 2965.97 | -13952.7 | 40936.6 | 10.34/96 |
| MD-V3 | -38.39 | 778.93 | -3698.88 | 7704.99 | 25.42/50 |

## 5. PROTON SPECTRUM FROM LASER ACCELERATION EXPERIMENTS

A stack configuration based on RCF layers can measure the divergence and energy spectrum of protons generated in laser-plasma interactions. In this type of configuration, RCF layers are interlaced with attenuators for a complete beam energy deposition in the stack, even at high energies. Each active layer corresponds to a specific energy of protons, namely the one given by the Bragg peak. The proton spectrum is deconvoluted with a minimization procedure starting from the deepest layers in the stack. As described in [19, 20] the total energy deposition in a given RCF layer is given by the expression:

$$E_{tot}(i) = \int \frac{\mathrm{d}N(E')}{dE} E_{dep}(i, E')\mathrm{d}E' \tag{7}$$

where d$N$/d$E$ is the energy spectrum and $E_{dep}$ is the energy loss by a proton with energy $E$, in a given layer of the stack. $E_{dep}$ can be estimated with a particle propagation code such as SRIM or Geant4 [18] for a given stack configuration and $E_{tot}$ for a given layer is compared with the experimental data in terms of optical density, since $E_{tot} = F$(OD), with the functional given by Eq. 6. Minimizing the difference between these two quantities one could obtain the expression of the energy spectrum dN/dE. In order to deliver this expression the procedure assumes an a-priori behavior of this parameter, different expressions are presented in [19, 21].

## 6. SUMMARY

In this work we reported a scattering experiment with monoenergetic protons delivered by an electrostatic accelerator at IFIN-HH for the calibration of two RCF types: HD-V2 and MD-V3. As a

consequence of the angular dependence of the scattering cross-section of the protons, the setup was able to provide a wide range of doses in a single run. In the analysis of the obtained data, we considered the main systematic uncertainties that influenced the results and we obtained calibration curves which will be used in a reconstruction of the proton beam from laser-plasma experiments in a stack configuration.

## ACKNOWLEDGEMENTS

We are grateful to G. Dumitru from Nuclear Physics Department (DFN) of IFIN-HH and V. Batrineanu and L. Povariu from Accelerators Department (DAT) of IFIN-HH for their important contributions in the setup realization and alignment. We also gratefully acknowledge the support from ELI-NP Phase II, a project co-financed by the Romanian Government and European Union through the European Regional Development Fund and the Competitiveness Operational Program (1/07.07.2016, COP, ID 1334).

## REFERENCES

1. http://www.ashland.com/industries/medical/medical-radiation-dosimetry/gafchromic-radiotherapy-films
2. P. BELLIDO et al., *Dosimetric Calibration of Radiochromic Film For Laser-accelerated Proton Beams*, 2013 IEEE Nuclear Science Symposium and Medical Imaging Conference, Seoul, 2013.
3. S. DEVIC et al., *Radiochromic Film as Dosimetric Tool for Low Energy Proton Beams*, Proceedings of Cyclotrons 2013, Vancouver, Canada, 2013.
4. A. S. CUCOANES et al., *On the potential of laser driven isotope generation at ELI-NP for positron emission tomography*, Medical Applications of Laser-Generated Beams of Particles IV: Review of Progress and Strategies for the Future, **B** 102390, 2017.
5. T. ASAVEI et al., *Materials in extreme environments for energy, accelerators and space applications at ELI-NP*, Rom. Rep. in Phys., **68**, Supp., S275S347, 2016.
6. J.GALY, J.MAGILL, R.SCHENKEL et al., *Nuclear Physics and Potential Transmutation with the Vulcan Laser*, Central Laser Facility Rutherford Appleton Laboratory, Annual Report 2001/2002, 2931, 2002.
7. M. BORGHESI et al., *Electric field detection in laser-plasma interaction experiments via the proton imaging technique*, Phys. Plasmas, **9,** 2214, 2002.
8. W. McLAUGHLIN et al., *Radiochromic Solid State Polymerization Reaction, Irradiation of Polymers*, American Chemical Society, 152166, 1996
9. A.S. CUCOANES, M. GUGIU, F. NEGOITA, F. ROTARU, M. TATARU, *A setup for multishot use of RCF stacks*, in preparation.
10. F. NEGOITA et al., *Laser driven nuclear physics at ELI-NP*, Rom. Rep. in Phys., **68**, Supp., S37S144, 2016.
11. A. AYDAROUS, M. EL GHAZALY, *Characterization of HD-V2 Gafchromic Film for Measurement of Spatial Dose Distribution from Alpha Particle of 5.5 MeV*, International Journal of Mathematical, Computational, Physical, Electrical and Computer Engineering V.**7**, 2013.
12. S. N. CHENETAL, *Absolute dosimetric characterization of Gafchromic EBT3 and HDv2 films using commercial flat-bed scanners and evaluation of the scanner response function variability*, Rev. of Sci. Instr., **87**, 073301, 2016.
13. D.G. GHITA et al., *Improvements of the research infrastructure at the tandem laboratory in IFIN-HH*, AIP Conf. Proc., **1525**, 208, 2013.
14. W. S. RASBAND, *ImageJ*, U.S. National Institutes of Health, Bethesda, Maryland, USA. See also: https://imagej.nih.gov/ij/
15. R. BRUNAND, F. RADEMAKERS, *ROOT-An Object Oriented Data Analysis Framework*, Proceedings AIHENP'96 Workshop, Lausanne, 1996; Nucl. Inst. & Meth. in Phys. Res. A, **389** 81-86, 1997. See also http://root.cern.ch/.
16. J. F. ZIEGLER, M. D. ZIEGLER, J. P. BIERSACK, *SRIM-The stopping and range of ions in matter*, Nucl. Inst. & Meth. in Phys. Res. B, **268**, 1818-1823., 2010.
17. J. W. MAYER, E. RIMINI, *Ion Beam Handbook for Material Analysis*, Academic Press, New York, 1977.
18. S. AGOSTINELLI, J. ALLISON, K. AMAKO et al., *Geant4 - a simulation toolkit*, Nucl. Inst. & Meth. In Phys. Res. A, **506**, 250303, 2003.
19. F. NURNBERG, M. SCHOLLMEIER et al., *Radiochromic film imaging spectroscopy of laser-accelerated proton beams*, Rev. Sci. Instr., **80**, 033301, 2009.
20. M. SCHOLLMEIER, M. GEISSEL, A.B. SEFKOW, K. A. FLIPPO, *Improved spectral data unfolding for radiochromic film imaging spectroscopy of laser-accelerated proton beams*, Rev. of Sci. Instr., **85**, 043305, 2014.
21. J. FUCHS, P. ANTICI, E..d'HUMIERES, *Laser-driven proton scaling laws and new paths towards energy increase*, Nature Phys., **2**, 48-54, 2006.

*Received March 15, 2018*